



Effect of fluid rheology on enhanced oil recovery in a microfluidic sandstone device



Michael A. Nilsson, Ruta Kulkarni, Lauren Gerberich, Ryan Hammond, Rohitashwa Singh, Elizabeth Baumhoff, Jonathan P. Rothstein*

Department of Mechanical and Industrial Engineering, University of Massachusetts Amherst, 160 Governors Drive, Amherst, MA 01003-2210, USA

ARTICLE INFO

Article history:

Received 26 February 2013
Received in revised form 24 September 2013
Accepted 29 September 2013
Available online 8 October 2013

Keywords:

Microfluidics
Enhanced oil recovery
Shear-thickening
Viscoelastic
Sandstone
Interfacial tension

ABSTRACT

As global energy usage increases, maximizing oil recovery from known reserves becomes crucial to meet the rising demand. In this work, we present the development of a microfluidic sandstone platform capable of quickly and inexpensively testing the performance of fluids with different rheological properties on the recovery of oil. Specifically, in this study we utilized these microfluidic devices to examine how shear-thinning, shear-thickening, and viscoelastic fluids affect oil recovery. Initial baseline experiments were performed by displacing oil with both water and a water–surfactant solution over a wide range of flow rates. The surfactant was found to reduce the interfacial tension of the water by a factor of ten and increased oil recovery by approximately 15% when compared to oil displaced by water at the same flow rates. Flopaam, a commercially available fluid thickener that is shear-thinning and viscoelastic was also studied. It was found to displace more oil than either the water or the surfactant solution and increase oil recovery at all flow rates studied. Finally, a shear-thickening nanoparticle solution was studied which was designed to thicken at a shear rate of approximately 10 s^{-1} . The shear rate corresponds to typical shear rates in the oil reservoirs, and values easily attainable in our microfluidic sandstone device. These shear-thickening fluids were found to be particularly effective at oil recovery. This was especially true for flowrates that closely matched the shear rates associated with the shear-thickening regime. When the appropriate choice of shear rate dependent viscosity was used to the capillary number, the oil recovery obtained from both the Newtonian and non-Newtonian was found to collapse quite well onto a single master curve. Additionally, it was shown that a two-stage recovery process that starts with an initial water flood followed by a flood with a secondary fluid can recover as much oil as a single stage recovery with that secondary fluid alone. These results clearly demonstrate that the microfluidic sandstone devices presented in this paper both reduce the time and cost required to investigate the effectiveness of enhanced oil recovery fluids using traditional methods, and can serve to quickly focus searches for customized oil recovery fluid selection.

© 2013 Elsevier B.V. All rights reserved.

1. Introduction

As the global oil supply decreases, the ability to effectively recover all of the oil from a particular well becomes increasingly important. The recovery of oil generally takes place in three stages: primary, secondary, and tertiary [1]. The primary stage occurs when the well is first accessed, and oil is produced by the internal pressures within the well. After completion of the primary stage, approximately 10% of the total oil in the field will have been recovered [1]. The secondary stage of oil recovery is characterized by the use of a driving or pumping fluid to displace oil in the reservoir. Generally water or a gas is employed as the driving fluid and typ-

ically results in an additional 20–40% of the original amount of the oil being recovered [1]. After primary and secondary oil recovery techniques have been exhausted, between 50% and 70% of the original oil remains in the oil field. It goes without saying then that there is an enormous amount of interest in developing methods to access and recover all of the remaining oil trapped within the reservoir. It is these tertiary or enhanced oil recovery (EOR) techniques that this paper will focus. Specifically, we investigate the role of the rheology of the driving fluid and shear thickening in particular on oil recovery.

The tertiary or enhanced stage of oil recover has developed much interest in more recent decades partially due to the rise in oil prices [1–7]. The goal of the tertiary stage is to be able to access and recover as much of the remaining oil in the fields as possible. The methods of tertiary oil recovery can be categorized into three

* Corresponding author.

E-mail address: rothstein@ecs.umass.edu (J.P. Rothstein).

main approaches: thermal, gas, and chemical. All three approaches aim to ease the recovery of the oil, either by changing the properties of the oil, the imbibing fluid, or the core material itself.

Chemical methods of enhanced oil recovery became widely popular during the 1980s [2]. Chemical methods aim to increase the amount of oil recovered by either increasing the effectiveness of water floods by modifying the water used to displace the oil, by reducing the interfacial tension between the imbibing fluid and the oil with the use of a host of different surfactants, or by modifying the wettability of the oil fields substrate to make it lyophobic [1,2,4]. Chemical methods use either alkali-polymers, surfactant polymers, or more recently a combination alkali-surfactant polymer system [2]. The larger challenge with chemical methods is that every possible variable with respect to fluid and substrate properties can change from one oil reservoir to the next and thus the chemistry must be tailored specifically for any given reservoir. There is a large body of work for conditions in and solutions to enhanced oil recovery in particular oil fields, summarized in a few works [2,7,8]. The main challenge resulting from the use of surfactants to lower the interfacial tension or polymers as a thickener is its delicate relationships to the conditions of the oil field substrate, which is not always constant, and the oil properties, which can also vary. Oftentimes, the polymers or surfactants are applied too far into the initial water flood, or they can lose effectiveness midway through the field [7]. Another challenge with chemical approaches to enhanced oil recovery is cost; depending on the fluctuating cost of oil and production, it can quickly become the prohibiting factor. While challenging, the vast amount of oil remaining within oil fields is only going to be a growing driving factor for EOR research as the easily-accessed oil is recovered and consumed. New fluid technologies will need developing, and modifications of existing technologies will need testing. In this paper, we study the impact of different rheological properties of the driving fluids using a series of microfluidic devices designed to mimic the physical and chemical properties of sandstone.

With a wide range of oil fields, testing methods are varied. It is impossible to perform *in situ* measurements. Instead, experiments are generally performed with core samples of the actual oil field extracted from the field. These samples can be filled with oil directly from the field, or similar man made oils. This core can then be used to test the ability of penetrating fluids to either displace the oil from pressure flow or imbibitions, which is where the displacing fluid wets the substrate by either natural wettability or by some alteration process [5]. This method does not allow for fine inspection of the processes at the pore and capillary level. Additionally, this method is prohibitively costly. This has led researchers towards the development of low cost alternatives.

Fluid testing is also performed on idealized representations of flows, often two-dimensional arrays of posts or cylinders or three-dimensional beds of packed spheres [5,9]. This allows for dimensions to be specified for precise control of particular fluid flow properties and examine dynamics at the micro- and nano-scales [5,9]. This method does not account for the inhomogeneous nature of field conditions or the true geometric flow constraints that exist in the field. Other researchers have used more complex micromodels to study multiphase flow in porous media composed of a network of channels etched into glass or fabricated in polymers [10–12]. These micromodels have proven to be extremely useful in studying a variety of enhanced oil processes because they provide direct visualization of a complex flow environment that can be easily modified to affect wettability, porosity or permeability. A nice literature survey on this topic can be found in Kamari et al. [12].

In this paper, a series of microfluidic devices were developed and used that were designed to precisely reproduce a two-dimensional slice from a sandstone core. Microfluidics is a relatively

young and developing field that encompasses the development of devices that allow for observations of fluid phenomena at the micro-scale [13–19]. In microfluidics, photolithography is used to transfer a pattern onto a silicon wafer using a photoresist such as SU-8 [20]. Once developed, the two-dimensional pattern in the photoresist is used as a master from which multiple daughters can be cast in polydimethyl-siloxane (PDMS) or other cross-linking polymers, containing negatives of the pattern on the master [14,21,22]. This soft lithography technique has been used for more than a decade to generate microfluidic devices containing features as small as 10 μm [22,23]. Here we utilize this technology to probe the effect of fluid rheology on oil recovery from hydrophobic microfluidic sandstone devices.

2. Experimental design

The device layout and properties are shown in Fig. 1. The mask was created from an actual cross-sectional image of sandstone which was used as a template for a microfluidic device that approximates flow through sandstone. The microfluidic device was fabricated out of PDMS using standard photolithographic techniques. The microfluidic sandstone device is 200 microns thick, and has capillaries and pores with average sizes from 200 microns to 10's of microns. The only modification to the sandstone that would affect the flow was that any "dead ends" were removed, and replaced with narrow passages. Even with these modest changes, we believe this design captures the essence of flow through sandstone using an easy-to-fabricate and extremely flexible experimental test bed.

The pressure ports allowed for the measurement of the pressure drop across the sandstone features. The ports were plumbed with blunt needle tips connected to polyethylene tubing. This tubing was connected through adapters to a differential pressure transducer (Honeywell TruStability™) with a range of ± 7 kPa. The pressure drop allows for the calculation of the permeability, $\kappa = U\eta\Delta x/\Delta P$, where U is the superficial velocity, η is the dynamic viscosity, Δx is the thickness of the medium, and ΔP is the pressure drop across the thickness. Common oilfields has permeability values of $0.1D < \kappa < 10.0D$. The pressure drop measured across the presented device resulted in a permeability value of $\kappa = 60D \pm 2D$. The porosity of the device is $\phi = 0.48$. While these values are slightly above the range of most oilfields [24], it is realistic in its structure, and its complexities allow for valuable insights in testing rheologically complex fluids.

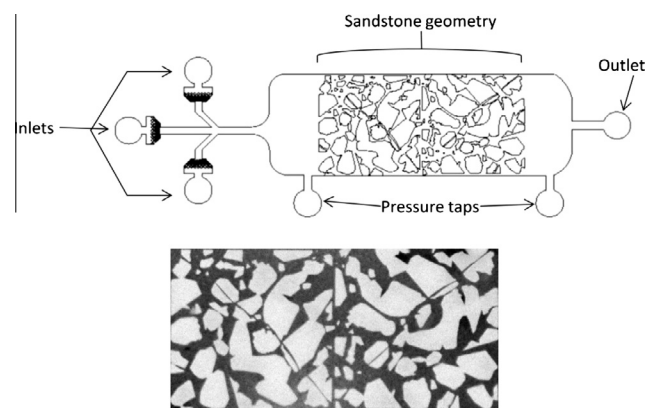


Fig. 1. Schematic diagram of the small sandstone device used in these experiments. The inlet is any of the three ports on the left, and flow goes from left to right. The two ports aside the main chamber are available for pressure drop measurements, and the port to the right is the outlet port. The lower image is what the sandstone portion looks like when filled with the Miglyol oil dyed with sudan blue.

In order to determine the amount of oil recovered, images were taken when the device was fully flooded with oil. To increase contrast with the PDMS, the oil was dyed with Sudan Blue (Sigma Aldrich), which is an oil-soluble coloring. A representative image of the fully oil-filled device is shown in Fig. 1. The original images were then compared against images of the flow cell at stages during and after the driving fluid had been pumped through the microfluidic device at a prescribed flowrate. In these experiments a syringe pump (kd Scientific, model 100) was used to impose a specific flow rate on the driving fluid. The experiment was terminated after it was determined that it had reached steady state. Steady state was defined as when no more oil was visibly being removed through the transparent exit tubing. The images were taken with a Nikon D70 camera outfitted with a macro-lens (micro-NIKKOR 105 mm). Backlighting was provided by a uniform light sheet (Dolan Jenner model QVABL) which was supplied by a light source (StockerYale Imagelite Model 20). The images were then made grayscale and imported into a homegrown Matlab™ code. The code first applied a threshold to each image, causing any oil filled area to appear completely black and any non-oil area white. The images were inspected to insure that the threshold value accurately represented the oil filled condition. The program then counted black pixels and reported the percentage of the image that was oil. Comparing between the percent of oil from the before and after the fluid flood allowed us to determine the percentage of oil removed during the flooding process.

The baseline fluid used to displace oil from within the microfluidic sandstone device is deionized water. The microfluidic devices are initially filled with Miglyol oil 840, a common oil used in cosmetics. Miglyol oil was chosen, amongst other reasons, because it does not significantly swell PDMS [25]. The viscosity of Miglyol oil was measured to be 10 mPa s. The interfacial tension between water and Miglyol oil 840 was measured using a pendant drop experiments and found to be $\sigma = 20$ mN/m. The advancing and receding contact angles between water and Miglyol oil wetted PDMS were measured using an optical goniometer and found to be $\theta_A/\theta_R = 160^\circ/144^\circ$. For all of the other driving fluids being used, we investigated variations in interfacial tension and fluid rheology.

In order to modify the interfacial tension without modifying viscosity, CTAB (hexadecyltrimethylammonium bromide) was added to the water phase at concentrations of 1 mM and 5 mM. At these concentration, which are larger than the critical micellar concentration (CMC) of 0.9 mM, there should be plenty of free surfactant in the bulk to fully populate the oil water interface [26]. Both CTAB solution reduced the equilibrium interfacial tension of water in Miglyol oil by an order of magnitude, from $\sigma = 20$ mN/m for pure water in oil to $\sigma = 2.1$ mN/m [25]. The contact angle between CTAB solution and Miglyol oil wetted PDMS was measured to be $\theta_A/\theta_R = 150^\circ/144^\circ$.

In order to increase the viscosity without affecting the interfacial tension, 15 wt% of a low molecular weight PEO ($M_w = 20,000$ g/mol, Aldrich) was added to water to create a Newtonian fluid with a shear viscosity of $\eta_0 = 140$ mPa s and an interfacial tension with Miglyol oil of $\sigma = 20$ mN/m that could be compared directly to the nanoparticle dispersions and the FloP-AAM solution. The advancing and receding contact angles with Miglyol oil wetted PDMS were found to be identical to water.

Modifying the viscosity of the driving fluid was achieved through the addition of nanoparticles and/or high and low molecular weight polymer additives to the water phase. Here we are interested in investigating the impact of two different rheological characteristics on enhanced oil recovery: shear thinning and shear thickening. The shear thickening fluid was created by adding a small amount (0.4 wt%) of a moderately high molecular weight polyethylene oxide (PEO) ($M_w = 600,000$ g/mol, Aldrich) to a nanoparticle solution of 4.0 wt% hydrophilic silica particles (12 nm size,

Degussa AEROSIL® 200). The shear rheology was measured using a cone-and-plate rheometer (TA Instruments, DHR-03) using a 40 mm 2° cone at 20 °C. As seen in Fig. 2, the nanoparticle dispersion initially shear thins. At a shear rate of $\dot{\gamma} = 10$ s⁻¹, the shear viscosity thickens by a factor of approximately forty. The fluid maintains this high viscosity until a shear rate of $\dot{\gamma} = 30$ s⁻¹ beyond which it begins to shear thin again. This shear thickening is induced by the interaction of nanoparticles enhanced by the presence of the polymer which can absorb to and bridge between nanoparticles to produce long-range interactions and a percolated network structure [27]. In the absence of polymers, the nanoparticle dispersions at this concentration show no shear thickening and a significantly reduced viscosity [27]. Small angle oscillatory shear measurements of this fluid do not reveal any elasticity over the range of shear rates that could be probed. The interfacial energy of the nanoparticle/polymer solution was found to be $\sigma = 20$ mN/m and the advancing and receding contact angles with PDMS in Miglyol oil were found to be $\theta_A/\theta_R = 159^\circ/143^\circ$.

Additionally, a commercially available viscoelastic fluid ‘thickener’, Flopaam 3630 (SNF Floerger®) was mixed with deionized water at a concentration of 0.1 wt%. Flopaam 3630 is a proprietary mixture of high molecular weight co-polymers of polyacrylamide and polyacrylate. At a concentration of 0.1 wt% Flopaam 3630, the mixture shows a zero shear rate viscosity of approximately

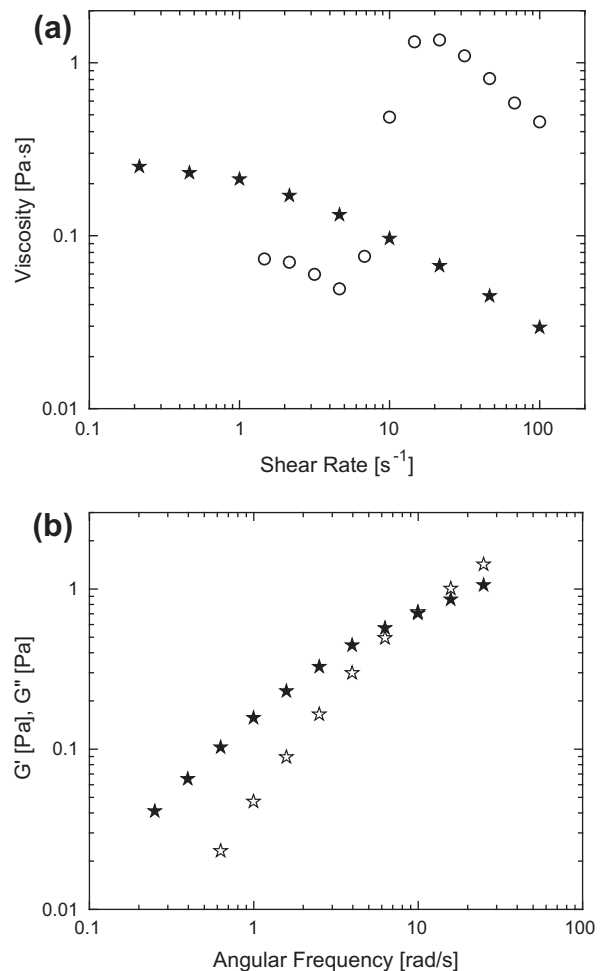


Fig. 2. (a) Viscosity as a function of shear rate for ★ 0.1 wt% Flopaam 3630 and the shear-thickening ○ 4.0 wt% silica nanoparticles 0.4 wt% PEO M_w 600,000. (b) The storage (G' , ★) and loss (G'' , ○) modulus as a function of angular frequency for the 0.1 wt% Flopaam 3630. The cross-over point is at 10 rad/s, corresponding to a relaxation time of $\lambda = 0.1$ s.

$\eta_0 = 250$ mPa s and shear thins over most of the range of shear rates probed. It was designed to have a viscosity in the same order of magnitude as the shear-thickening nanoparticle dispersion over the range of interesting shear rates. As seen in Fig. 2a, the viscosity of the 0.1 wt% Flopaam 3630 shear thins at roughly the same rate as the shear thickening nanoparticle dispersion. There are two major differences between these fluids. First, the Flopaam does not shear thicken. Second, as seen in Fig. 2b, the linear viscoelastic spectrum of Flopaam shows the fluid to be viscoelastic with a relaxation time of $\lambda = 0.1$ s. The interfacial energy of the Flopaam solution was found to be $\sigma = 20$ mN/m and the advancing and receding contact angles with PDMS in Miglyol oil were measured to be $\theta_A/\theta_R = 159^\circ/144^\circ$. Note that there is very little variation in the contact angles measured for all these fluids so differences in oil recovery should be just a function of fluid rheology and interfacial tension.

3. Results and discussion

The most common driving fluid used for oil recovery is water. Thus, for this study, water is used as the control for which other driving fluids are compared against. The flowrates of driving water through the microfluidic sandstone device ranged between 1.5 ml/h and 22 ml/h. This corresponds to front speeds just before the sandstone features of 0.38–5.5 mm/s and capillary numbers for water that ranged between $3.8 \times 10^{-5} < Ca = \eta U/\sigma < 5.6 \times 10^{-3}$. The results for water and the other driving fluids are presented in Fig. 3. In Fig. 3, the percentage of oil remaining in the microfluidic sandstone device after the flow has reached steady state is presented as a function of the flow rate of the driving fluid. Steady state was achieved when no oil drops could be observed in the outlet tubing and no movement of oil was observed within the microfluidic sandstone device. At the lowest flowrates tested, approximately 65% of the oil remained after flooding with water at 1.5 ml/h. As the flowrate was increased, more oil was recovered until the data approached an asymptotic value of roughly 40% residual oil at large flowrates. The general trend of increasing oil recovery with increasing flowrate or capillary number has been observed many times in the past [5,7,9,28,29].

Rather than simply increasing the front velocity, two alternative approaches to increasing the capillary number is to decrease the interfacial tension or increase the shear viscosity of the driving fluid. The 5 mM CTAB solution has a lower interfacial tension than water but has the same viscosity. The 15 wt% PEO solution has the same interfacial tension, but a larger viscosity. As seen Fig. 3a, the CTAB solution recovers approximately 15% more oil than water at every flowrate investigated while the Newtonian PEO solution improves the oil recovery even more. The lower interfacial tension reduces the Laplace pressure that must be overcome if the driving fluid is to displace the oil while the higher shear viscosity increases the pressure throughout the sandstone device. This is especially true in regions of higher interfacial curvature like entrances to narrow capillaries from larger pores. As one can see, when the data is recast as a function of capillary number, as seen in Fig. 3b, the water, 5 mM CTAB and Newtonian PEO data appear to collapse reasonably well onto a single master curve.

This result is expected for hydrophilic, water wetting rock, but not necessarily for hydrophobic, oil wetting rock when the driving fluid contains surfactants. This is because of the shearing and continuous generation of the surfactant-laden oil–water interface. For two phase flow through channels and Hele Shaw cells, it has been shown that if the displacing fluid does not wet the channel, as it flows into the displaced fluid it can leave behind a very thin film of oil on all the walls. This film is often thin enough that it is not easily imaged in either a Hele Shaw cell or our microfluidic

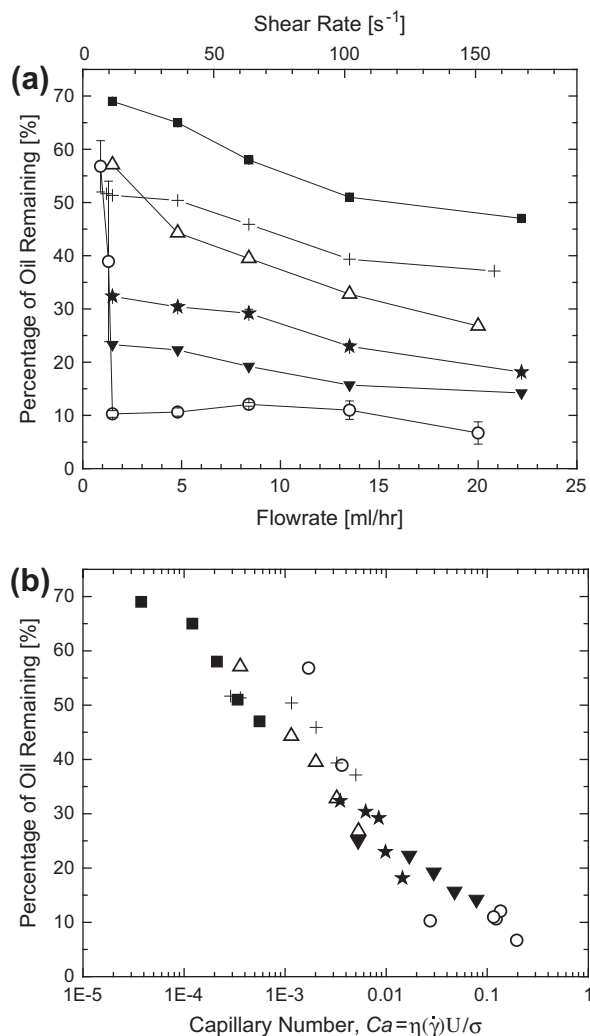


Fig. 3. (a) The percent oil remaining in the sandstone microfluidic device after flooding with various fluids as a function of flowrate. (b) The percent oil remaining in the sandstone microfluidic device after flooding with various fluids as a function of capillary number. The driving fluids in both include: ■ water, △ 5 mM CTAB in water surfactant solution, ▼ 15 wt% low Mw PEO in water, +1 mM CTAB in water surfactant solution, ○ shear thickening fluid consisting of 4.0 wt% silica nanoparticle 0.4 wt% PEO M_w 600,000 in water, and ★ 0.1 wt% Flopaam 3630 in water.

sandstone device after flooding. The thickness of that oil film in a Hele Shaw cell was predicted by Park and Homsy to scale with $Ca^{2/3}$ [30,31]. As a result, new interface is produced continuously as the displacing fluid moves into our sandstone device. When using a surfactant solution as the driving fluid, the newly created oil–water interface must be populated by surfactant. This takes a finite amount of time which depends on the diffusion coefficient and concentration of the surfactant as well as the rate of adsorption to the interface [32,33]. Until the newly formed oil–water interface is fully populated by surfactant, its interfacial tension can be much larger than the equilibrium value measured by a pendant drop experiment. Additionally, as the surfactant solution moves through the sandstone device the surfactant populating the leading edge of the advancing fluid front experiences a shear flow that can sweep the surfactant from the leading edge upstream, locally reducing the surfactant concentration and increasing the interfacial tension along the oil–water interface [32,33]. As a result, the true capillary number may be significantly smaller than that calculated using the equilibrium value of the interfacial tension. Bonn et al. [32,33] demonstrated that gradients in surfactant concentration along an oil–water interface in two phase flow

through a Hele-Shaw cell could explain the failure of viscous fingering data to collapse with capillary number.

In our initial experiments, the concentration of CTAB in the surfactant solution was chosen to be five times larger than the CMC, 5 mM, so that the concentration of free surfactant in the bulk was large enough to quickly populate any new interface generated during oil recovery. The resulting data for the 5 mM case collapse with capillary number very well onto a single master curve with water and the high viscosity Newtonian PEO solution. However, by reducing the CTAB concentration from 5 mM to just above the CMC at 1 mM, the impact of interfacial tension gradients on the oil recover can be observed in Fig. 3b. The 1 mM CTAB solution has the same equilibrium surface tension as the 5 mM solution, but five times fewer surfactant molecules in bulk available to populate depleted or newly generated oil–water interface. At the lowest flow rates studied, the 1 mM data was found to collapse quite nicely with capillary number onto the result for water and the 5 mM CTAB solution. However, as the capillary number and the strength of the shear flow were increased, a shift in the data to the right by a factor of roughly three was observed in Fig. 3b. These observations are consistent with the trends observed by Bonn et al. [32,33] and clearly demonstrate that, for oil recovery from hydrophobic rock using surfactant solutions, variations in interfacial tension can result in the failure of oil recovery data to collapse with capillary number.

The shear thickening nanoparticle/PEO fluid recovered more oil than either the water or the CTAB solution in oil recover at flowrates between 1.5 and 22 ml/h. At the lowest flowrates tested, 0.9 ml/h, the shear-thickening fluid roughly matches the oil recovery obtained using the surfactant solution. This is a due to the large viscosity of the nanoparticle solution even prior to shear thickening increasing the capillary number as seen in Fig. 3b. At flowrates above approximately 1 ml/h, a dramatic improvement in the oil recovery is observed, peaking at a flow rate of 1.5 ml/h with just 14% of the oil remaining in the microfluidic sandstone device at steady state. As the flowrate was increased, the shear-thickening fluid was found to recover significantly more oil than the water, surfactant solution, and the high viscosity Newtonian PEO solution at the same flow rates. An important question to ask is whether the data for the shear thickening fluid will collapse with capillary number. In order to evaluate the capillary number, the correct value of the viscosity must be determined. The simplest choice is to use a constant value of viscosity. However, if one chooses the zero shear rate viscosity of the shear thickening solution, which is approximately $\eta_0 = 80$ mPa s, the data do not collapse with capillary number onto the master curve in Fig. 3b produced by the Newtonian fluids tested previously. This can be seen most clearly when compared to the high viscosity Newtonian PEO solution. Even though the PEO solution has a larger viscosity, $\eta_0 = 140$ mPa s, at the highest flow rates tested the shear thickening solution still removes considerably more oil. The effect of shear thickening must be taken into account by evaluating the capillary number using the correct value of the shear rate dependent viscosity such that $Ca = \eta(\dot{\gamma})U/\sigma$.

To obtain a better understanding of the underlying physics at work with a shear thickening fluid, the oil recovery data is also plotted as a function of shear rate in Fig. 3a. For flow through a rectangular channel, the shear rate depends on aspect ratio [ref white]. The device has a mean pore opening size of $W = 200$ μm , and is $H = 200$ μm . The average front speed is calculated as, $U = Q/\phi HL$, where Q is the volume flow rate, $L = 5.7$ mm is the overall width of the device and ϕ is the porosity of the sandstone. It has been shown that for flow through a square channel that the wall shear rate becomes approximately $\dot{\gamma}_w \cong 6U/W$ [34,35]. The shear rate across the channel, however, is not constant so the average shear rate in the square channel, $\dot{\gamma} = 3U/W$, was chosen as a characteristic shear rate in the sandstone device in order to evaluate

the viscosity of the shear thickening fluid [34]. As seen in 3a, the onset of improved oil recovery coincides with the shear rates of approximately $\dot{\gamma} \approx 7$ s^{-1} . This shear rate corresponds very well with the critical shear rate for the onset of shear thickening observed in the steady shear rheology measurements in Fig. 2. If the shear rate dependent viscosity is used to evaluate the capillary number, the data appears to collapse reasonably well onto the master curve developed from the results from the Newtonian fluids in Fig. 3b although some deviations are observed at the lowest capillary numbers. This is likely the result of the variation in flow rate and shear rate across the complex interconnected channels within our microfluidic sandstone device and the simplifying assumption of a constant shear rate used to evaluate the viscosity.

These observations suggest quite strongly that the increased pressure drop resulting from the shear-thickening transition is sufficient to overcome the Laplace pressure supporting water–oil interfaces in small capillaries and side branches. Once the capillaries are opened, a larger fraction of the sandstone device is accessed by the driving fluid and as a result the local shear rate is reduced. In some cases, the reduced shear rate can drive the viscosity back below the shear thickening transition, reducing the pressure drop in the oil-depleted portions of the sandstone device. While the oil recovery increases with the onset of the shear-thickening, the peak oil recovery was found to exist over a wide range of average shear rates that extend past the maximum in the shear viscosity and well into the shear thinning regime at high shear rates where the viscosity remains high and the resulting capillary number is still quite large.

It is important to note that there exists uncertainty in these experiments that result from small variations in fluid preparations and the device fabrication. The shear-thickening behavior is very sensitive in the small variations in fluid composition. The device fabrication can also result in small variations in the thickness of the capillaries and pores, which would affect the shear-thickening onset. In order to minimize the effect of these variations, the experiments were performed using multiple independently prepared fluid samples and device fabrications. Error bars are presented to demonstrate the confidence in these results.

As seen in Fig. 3a, at a given flow rate, the viscoelastic Flopaam 3630 mixture was found to recover more oil than both the water and the CTAB solution, and followed the same general trend of increasing oil recovery with increasing flowrate even though the viscosity was found to thin over the entire range of shear rates tested. The Flopaam solution was also found to recover more oil than the shear thickening fluid in regions far outside of the shear rates where the thickening occurs. This is important, as it demonstrates that by designing a fluid that thickens at a target shear rate, oil recovery can exceed that of current enhanced oil recovery fluids in use today. When the data is recast in terms of a shear rate dependent capillary number, as seen in Fig. 3b, it is again found to collapse onto the master curve quite well. Thus it appears that for both Newtonian and non-Newtonian fluids, if one can determine an appropriate shear rate dependent viscosity, the global oil recovery measurements depends only on the shear rate dependent capillary number. However, even though the global oil recovery results appear to be similar, by interrogating in detail the images taken before and after flooding with each of the driving fluids differences in the local mobilization of oil can be observed.

By performing a detailed examination of the images used for determining the oil recovery, it is possible to qualitatively assess regions where one particular fluid outperforms others in accessing and mobilizing the trapped oil. Fig. 4 compares three before and after images of oil recovery experiments performed at a flowrate of 4.8 ml/h. The initial oil-filled sandstone is shown in Fig. 4a. The steady state result for water is shown in Fig. 4b. The water is observed to form canals that cuts through the most permeable

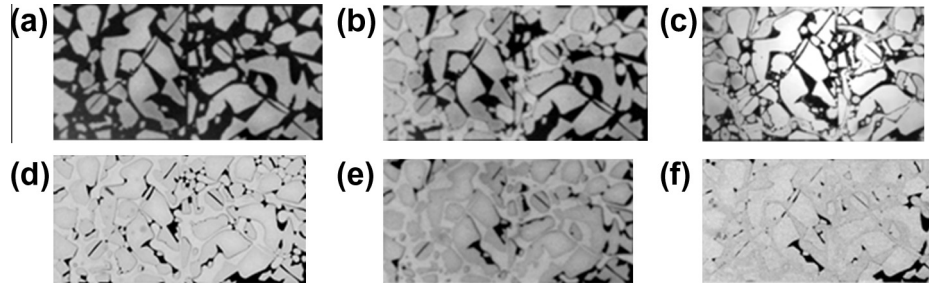


Fig. 4. (a) The initial microfluidic sandstone geometry filled with Miglyol oil dyed with Sudan blue. The oil-filled microfluidic sandstone device is shown after reaching steady-state by single-stage flooding at 4.8 ml/h with (b) water, (c) 5 mM CTAB in water surfactant solution, (d) 15 wt% low Mw PEO in water, (e) 0.1 wt% Flopaam 3630 in water, and (f) shear thickening fluid consisting of 4.0 wt% silica nanoparticle 0.4 wt% PEO M_w 600,000 in water. The width (top to bottom in image) of each device is $L = 5.68$ mm.

areas of the sandstone and allows additional water to flow through, with occasional drops of water pinching off in smaller capillaries and pores alongside the main canals. As one progresses across different driving fluids from Fig. 4b–f, more and more oil is recovered from the sandstone. This can be seen most clearly for the viscoelastic Flopaam solution and the shear thickening fluid in Fig. 4e and f, where the comparisons to the water case are quite striking. Nearly all the oil in these two cases has been recovered. These observations should not be surprising because although the images in Fig. 4 are presented at the same flow rates, the capillary numbers vary by several orders of magnitude from Fig. 4b–f. It is thus important to compare images for the viscoelastic Flopaam 3630 with the shear thickening nanoparticle dispersion at the same capillary number.

In Fig. 5, a comparison between water, the shear-thickening fluid, and the Flopaam solution is shown for flow rates of 1.5 ml/h, 4.8 ml/h, 8.4 ml/h, and 13.5 ml/h. The corresponding capillary numbers are presented in the figure caption. In all cases, one observes an increase in oil recovery with an increase in flow rate and capillary number. Within Fig. 5, it is possible to compare the results for Flopaam and the shear thickening fluid at roughly the same capillary number by comparing the oil recovered in the

images in Fig. 5b and i. What one observes is that there are a number of distinct differences that emerge even though the overall oil recovery is quite similar. Specifically, the shear thickening fluid appears to be more successful at mobilizing oil from small capillaries. Additionally, the viscoelastic fluid appears to be more successful at accessing oil from within dead-end pores and unswept volumes. These effects likely result from the elasticity of the Flopaam 3630 solution, which has a relaxation time of approximately $\lambda = 0.1$ s. For all the experiments presented in Fig. 5, the average shear rate is large enough that the Weissenberg number is greater than one $Wi = \dot{\gamma}\lambda > 1$ and the elastic effect will be important. As the fluid passes from a pore into a capillary, an extensional flow is produced followed by a strong shear flow within the capillary. Flow into and through the capillaries result in the deformation of the polymer chains in the flow direction and the buildup of significant elastic normal stresses [36]. Upon exiting of the capillaries, some of the elastic stress is released as the polymer partially recoils back towards its equilibrium configuration. Much like die swell during extrusion of polymeric fluids [37,38], the elastic normal stresses within the Flopaam drive the fluid quickly outward to fill the pores it is entering. As a result, the Flopaam can access more oil from dead-end pores as seen in Fig. 5.

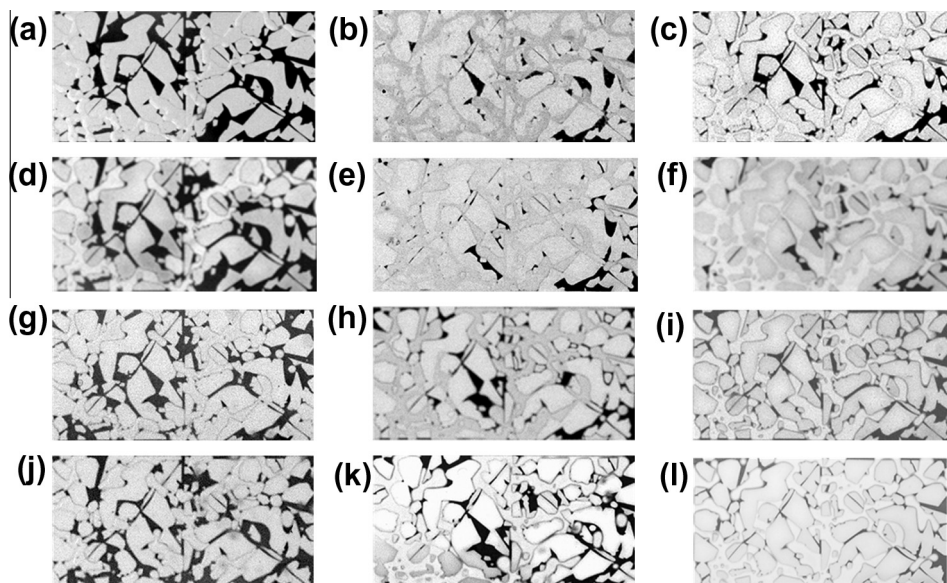


Fig. 5. The oil-filled microfluidic sandstone device is shown after reaching steady-state by single-stage flooding with (a) water at 1.5 ml/h ($Ca = 3.7 \times 10^{-5}$), (b) shear-thickening fluid at 1.5 ml/h ($Ca = 0.027$), (c) Flopaam solution at 1.5 ml/h ($Ca = 0.0035$), (d) water at 4.8 ml/h ($Ca = 1.2 \times 10^{-4}$), (e) shear-thickening fluid at 4.8 ml/h ($Ca = 0.12$), (f) Flopaam solution at 4.8 ml/h ($Ca = 0.0062$), (g) water at 8.4 ml/h ($Ca = 2.1 \times 10^{-4}$), (h) shear-thickening fluid at 8.4 ml/h ($Ca = 0.13$), (i) Flopaam solution at 8.4 ml/h ($Ca = 0.0084$), (j) water at 13.5 ml/h ($Ca = 3.4 \times 10^{-4}$), (k) shear-thickening fluid at 13.5 ml/h ($Ca = 0.116$), and (l) Flopaam solution at 13.5 ml/h ($Ca = 0.010$). The width (top to bottom in image) of each device is $L = 5.68$ mm.

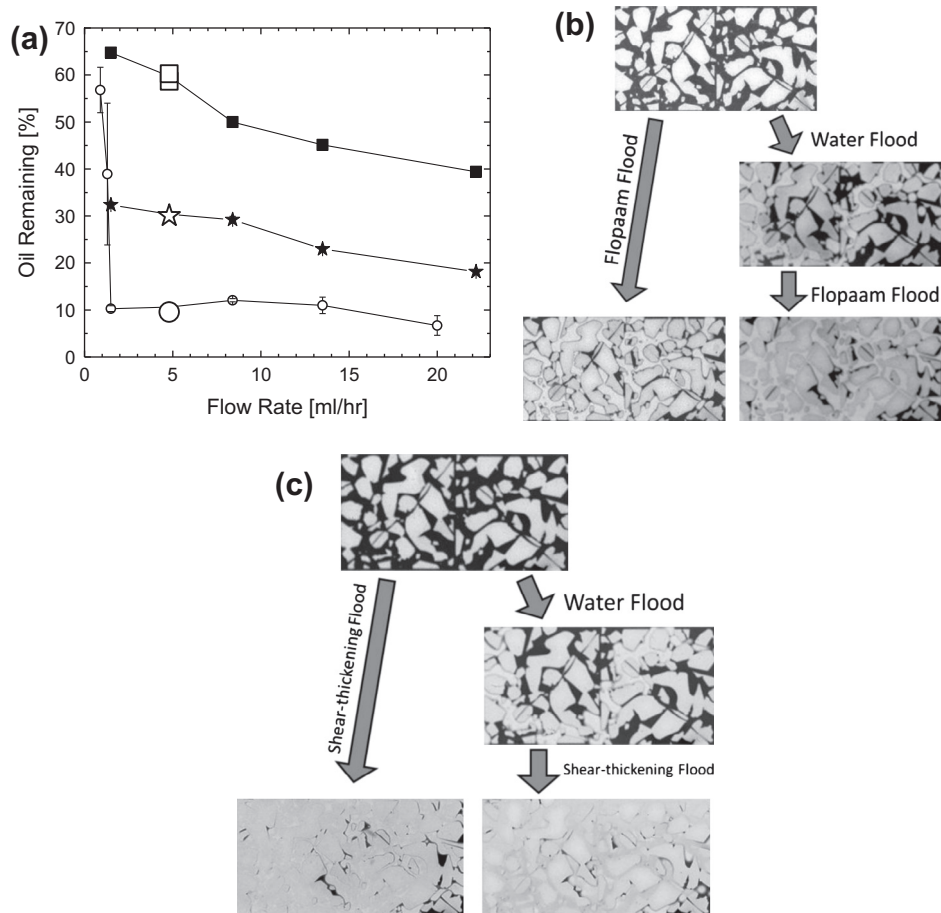


Fig. 6. (a) The percent oil remaining as a function of flowrate for ■ water, ○ shear-thickening solution, and ★ Flopaam 3630. The stars indicate two stage recovery residual oil, starting with a □ water flood, the secondary (larger ○) shear-thickening solution, and the secondary ☆ Flopaam flood. (b) The initial oil filled microfluidic sandstone geometry and comparing the steady-state results after flooding with only the Flopaam 3630 solution against flooding first with water and a secondary flood with the Flopaam solution. (c) The initial oil filled microfluidic sandstone geometry and comparing the steady-state results after flooding with only the shear-thickening nanoparticle solution against flooding first with water and a secondary flood with the shear-thickening solution.

Finally, an important consideration is the ability of an enhanced oil recovery driving fluid to recover additional oil out of a field previously flooded with water for second stage recovery. Our microfluidic sandstone devices were designed with multiple inlets to make sequential flooding experiments easy to perform. The results for sequential flooding with water followed by Flopaam and the shear thickening fluid are shown in Fig. 6. At a flowrate of 4.8 ml/h, water was initially used to flood the microfluidic sandstone device. The amount of oil recovered from initially flooding of the small sandstone device with water matches the average from multiple single flood measurements in Fig. 3. This data is shown as an open square overlaid on the data in Fig. 6a. Fig. 6b shows the results of subsequently pumping the Flopaam mixture through at the same flowrate (4.8 ml/h) until steady state was obtained. Interestingly, the secondary fluid managed to recover exactly the same amount of oil as was obtained by the single flood with the Flopaam. The net residual oil of the Flopaam 3630 two-stage flood is represented by the open star in Fig. 6a. This indicates that an initial flood of water does not significantly affect the overall recover in a two stage flooding. Another interesting point is that with the initial water flood, the water forms a path of lower viscosity the oil, but the subsequent Flopaam solution flood does not show preferential flow through that path. The resulting images shown in Fig. 6b are largely similar, with a few noticeable differences. The device only flooded with Flopaam had many dead-end pores nearly empty of oil and the second stage Flopaam flood did not remove as much oil from those pores. However, the second

stage Flopaam flood did remove more oil from some of the smaller capillaries that the single stage Flopaam flood did not. Additionally, The Flopaam in the second stage flood was able to connect across some capillaries where water had been where the single stage Flopaam could not. This indicates that there are some preferential flow paths at smaller scales that a first stage water flood might enable the Flopaam to access. Fig. 6c compares the result of the two-stage flooding process flooding with water first and following with the shear-thickening fluid to the result of a single stage flood using the shear-thickening fluid. The results of the two-stage flood agree extremely well with the result of a single stage flood using the shear-thickening fluid. The two-stage residual oil is represented by the open circle in Fig. 6a. The only differences apparent between a single stage and two-stage flood with the shear-thickening fluid are some small areas where water helped mobilize oil in the two-stage flood that remain in the single stage flood. Even with these obvious differences, the overall oil recovery remains very similar between a single stage Flopaam or shear-thickening flood and their two-stage counterpart floods that flood with water before flooding with the Flopaam or shear thickening fluid.

4. Conclusions

Enhanced oil recovery is an increasingly important field, and this work presents the efforts of developing a microfluidic platform for quickly testing fluids of different rheological properties for the

recovery of oil from hydrophobic sandstone. Water was tested in the microfluidic sandstone device as a baseline for oil recovery comparison. Systematic variations of fluid properties were examined for their ability to increase oil recovery. A 5 mM CTAB surfactant solution was mixed in order to lower the interfacial tension with the Miglyol oil used by a factor of ten. The surfactant solution was found to increase the recovered oil by about 15% over the range of flowrates tested. A number of non-Newtonian EOR fluids were also tested. The first, was a commercially available fluid thickener, Flopaam, designed specifically for enhanced oil recovery. The Flopaam solution was shear-thinning and viscoelastic and found to recover more oil than both the surfactant solutions and water at all flowrates tested. A shear thickening fluid containing a mixture of 0.6 wt% high molecular weight PEO and 4wt% fumed silica nanoparticles was also tested. The nanoparticle dispersion was designed to shear thicken at shear rates typical of oil fields and present in the microfluidic sandstone devices used in these experiments. This shear thickening fluid achieved more oil recovery than the water, surfactant, and Flopaam solutions for flowrates that closely matches the shear thickening regime.

When the data was recast as a function of capillary number, where the viscosity was evaluated at a representative shear rate within the microfluidic sandstone device, all the data sets were found to collapse quite well to a single master curve. Thus it appears that the changes in oil recovery can be understood quite well for non-Newtonian fluids if one fully characterizes the rheological properties of the fluid. It was demonstrated that a two-stage recovery process using water and a secondary fluid can recover as much oil as a single stage recovery with the secondary fluid. The microfluidic sandstone device was thus proven to be a relative quick diagnostic tool to investigate the ability of enhanced oil recovery fluids to be tested for effectiveness before more costly and time intensive methods are employed. Future work with larger, more complex, lower permeability microfluidic sandstone devices are ongoing and will be reported on in the near future [39]. Finally, for oil field applications, shear-thickening fluids show great promise for enhanced oil recovery in the future.

Acknowledgements

The authors would like to acknowledge BASF for their financial support of this work, as well as Jack Tinsley, Christian Kunkelmann, Sebastian Weisse, Ravindra Aglave, and Björn Heinz for their assistance and enlightening discussions.

References

- [1] U.S. Department of Energy, Enhanced Oil Recovery/CO₂ Injection, U.S. Department of Energy, Washington, DC, 2011.
- [2] V. Alvarado, E. Manrique, Enhanced oil recovery: an update review, *Energies* 3 (2010) 1529–1575.
- [3] A.R. Brandt, S. Unnasch, Energy intensity and greenhouse gas emissions from thermal enhanced oil recovery, *Energy and Fuels* 24 (2010) 4581–4589.
- [4] S.J. Fathi, T. Austad, S. Strand, Water-based enhanced oil recovery (EOR) by “Smart Water”: optimal ionic composition for EOR in carbonates, *Energy and Fuels* 25 (2011) 5173–5179.
- [5] B.Y. Jamaloei, R. Kharat, K. Asghari, Pore-scale events in drainage process through porous media under high- and low-interfacial tension flow conditions, *Journal of Petroleum Science and Engineering* 75 (2010) 223–233.
- [6] R.B. Needham, P.H. Doe, Polymer flooding review, *Journal of Petroleum Technology* 39 (1987) 1503–1507.
- [7] S. Thomas, Enhanced oil recovery – an overview, *Oil and Gas Science and Technology-Revue De L Institut Francais Du Petrole* 63 (2008) 9–19.
- [8] D.A.Z. Wever, F. Picchioni, A.A. Broekhuis, Polymers for enhanced oil recovery: a paradigm for structure–property relationship in aqueous solution, *Progress in Polymer Science* 36 (2011) 1558–1628.
- [9] R.P. Chhabra, *Bubbles, Drops and Particles in Non-Newtonian Fluids*, CRC Press, Boca Raton, 2007.
- [10] S.G. Sayegh, D.B. Fisher, Enhanced oil recovery by CO₂ flooding in homogeneous and heterogeneous 2D micromodels, *Journal of Canadian Petroleum Technology* 48 (2009) 30–36.
- [11] M. McKellar, N.C. Warelaw, A method of making two-dimensional glass micromodels of pore systems, *Journal of Canadian Petroleum Technology* 21 (1982) 39–41.
- [12] E. Kamari, D. Rashtchian, S.R. Shadizadeh, Immiscible displacement of awetting fluid by a non-wetting one at high capillary number in a micro-model containing a single fracture, *Transport in Porous Media* 94 (2012) 289–301.
- [13] J. Atencia, D.J. Beebe, Controlled microfluidic interfaces, *Nature* 437 (2005) 648–655.
- [14] D.C. Duffy, J.C. McDonald, O.J.A. Schueller, G.M. Whitesides, Rapid prototyping of microfluidic systems in poly(dimethylsiloxane), *Analytical Chemistry* 70 (1998) 4974–4984.
- [15] L.C. Gao, T.J. McCarthy, An “artificial lotus leaf” prepared using a 1945 patent and a commercial textile, *Abstracts of Papers of the American Chemical Society* 231 (2006).
- [16] Z.H. Nie, M.S. Seo, S.Q. Xu, P.C. Lewis, M. Mok, E. Kumacheva, G.M. Whitesides, P. Garstecki, H.A. Stone, Emulsification in a microfluidic flow-focusing device: effect of the viscosities of the liquids, *Microfluidics and Nanofluidics* 5 (2008) 585–594.
- [17] K.E. Petersen, Silicon as a mechanical material, *Proceedings of the Ieee* 70 (1982) 420–457.
- [18] H.A. Stone, A.D. Stroock, A. Ajdari, Engineering flows in small devices: microfluidics toward a lab-on-a-chip, *Annual Review of Fluid Mechanics* 36 (2004) 381–411.
- [19] G.M. Whitesides, The origins and the future of microfluidics, *Nature* 442 (2006) 368–373.
- [20] M.J. Madou, *Fundamentals of Microfabrication: The Science of Miniaturization*, CRC Press, Boca Raton, Fla., 2002.
- [21] J.C. McDonald, D.C. Duffy, J.R. Anderson, D.T. Chiu, H.K. Wu, O.J.A. Schueller, G.M. Whitesides, Fabrication of microfluidic systems in poly(dimethylsiloxane), *Electrophoresis* 21 (2000) 27–40.
- [22] J.C. McDonald, G.M. Whitesides, Poly(dimethylsiloxane) as a material for fabricating microfluidic devices, *Accounts of Chemical Research* 35 (2002) 491–499.
- [23] H. Makamba, J.H. Kim, K. Lim, N. Park, J.H. Hahn, Surface modification of poly(dimethylsiloxane) microchannels, *Electrophoresis* 24 (2003) 3607–3619.
- [24] D. Han, A. Nur, D. Morgan, Effects of porosity and clay content on wave velocities in sandstones, *Geophysics* 51 (1986) 2093–2107.
- [25] M.K. Mulligan, J.P. Rothstein, The effect of confinement-induced shear on drop deformation and breakup in microfluidic extensional flows, *Physics of Fluids* 23 (2011) 022004.
- [26] J.N. Israelachvili, *Intermolecular and Surface Forces: With Applications to Colloidal and Biological Systems*, Academic Press, London, 1985.
- [27] M. Kamibayashi, H. Ogura, Y. Otsubo, Shear-thickening flow of nanoparticle suspensions flocculated by polymer bridging, *Journal Colloid and Interface Science* 321 (2008) 294–301.
- [28] C. Cottin, H. Bodiguel, A. Colin, Drainage in two-dimensional porous media: from capillary fingering to viscous flow, *Physical Review E* 82 (2010).
- [29] J.J. Taber, Research on enhanced oil-recovery – past, present and future, *Pure and Applied Chemistry* 52 (1980) 1323–1347.
- [30] G.M. Homsy, Viscous fingering in porous media, *Annual Review of Fluid Mechanics* 19 (1987) 271–311.
- [31] C.W. Park, G.M. Homsy, Two-phase displacement in Hele Shaw cells: theory, *Journal of Fluid Mechanics* 139 (1984) 291–308.
- [32] D. Bonn, H. Kellay, J. Meunier, Viscous fingering and related instabilities in complex fluids, *Philosophical Magazine B* 78 (1998) 131–142.
- [33] D. Bonn, H. Kellay, M.B. Amar, J. Meunier, Viscous finger widening with surfactants and polymers, *Physical Review Letters* 75 (1995) 2132–2135.
- [34] Y. Son, Determination of shear viscosity and shear rate from pressure drop and flow rate relationship in a rectangular channel, *Polymer* 48 (2007) 632–637.
- [35] F.M. White, *Viscous Fluid Flow*, McGraw-Hill, New York, 1991.
- [36] J.P. Rothstein, G.H. McKinley, The axisymmetric contraction–expansion: the role of extensional rheology on vortex growth dynamics and the enhanced pressure drop, *Journal of Non-Newtonian Fluid Mechanics* 98 (2001) 33–63.
- [37] R.G. Larson, Instabilities in viscoelastic flows, *Rheologica Acta* 31 (1992) 213–263.
- [38] C.J.S. Petrie, M.M. Denn, Instabilities in polymer processing, *Aiche Journal* 22 (1976) 209–236.
- [39] M.A. Nilsson, *Multiphase Flows with Digital and Traditional Microfluidics*, Ph.D. Thesis, University of Massachusetts – Amherst, 2013.